Dynamics and structure in the Mn2+ site of concanavalin A as determined by high-field EPR and ENDOR spectroscopy

3 AUTHORS, INCLUDING:

Kv Narasimhulu
Tampa, USA

46 PUBLICATIONS **885** CITATIONS

SEE PROFILE

Raanan Carmielli
Weizmann Institute of Science

44 PUBLICATIONS **866** CITATIONS

SEE PROFILE

MRC

Dynamics and structure in the Mn²⁺ site of concanavalin A as determined by high-field EPR and ENDOR spectroscopy†

Daniella Goldfarb,* Kuppala V. Narasimhulu and Raanan Carmieli

Departments of Chemical Physics, The Weizmann Institute of Science, Rehovot Israel 76100

The properties of the Mn²⁺ site in the protein concanavalin A were investigated by single crystal W-band EPR/ENDOR (electron-nuclear double resonance) measurements. Initially, room temperature EPR measurements were carried out, one type of Mn²⁺ was identified and its zero-field splitting (ZFS) tensor was determined. In contrast, low temperature EPR measurements showed that two chemically inequivalent Mn²⁺ are present, Mn_A^{2+} and Mn_B^{2+}, differing in their ZFS tensors. Variable temperature measurements revealed a two-site exchange between the two types. Although the dynamic process has been characterized by its rate and activation energy, just from the EPR measurements it was not possible to assign it to a specific residue. ¹H ENDOR measurements of the water and imidazole protons, which are the main contributors to the ENDOR spectra, showed only one type of signals, namely, they were not sensitive to the differences between Mn_A^{2+} and Mn_B^{2+}. ⁵⁵Mn ENDOR spectra, which are dominated by the ⁵⁵Mn isotropic hyperfine, a_{iso}, and the nuclear quadrupole interaction did sense the differences. Analysis of the spectra recorded with the magnetic field along the crystallographic axes showed that the two have the same a_{iso} but different quadrupole tensors. Copyright © 2005 John Wiley & Sons, Ltd.

KEYWORDS: EPR; ENDOR; high field; single crystal; concanavalin A; conformational dynamics

INTRODUCTION

Electron paramagnetic resonance (EPR) and electron-nuclear double resonance (ENDOR) are among the best techniques used to characterize paramagnetic metal ion centers in metalloenzymes and proteins. Most often the sample under study is a frozen solution of which the EPR/ENDOR spectra are governed by the anisotropy of the magnetic interactions. This anisotropy is essential for obtaining electronic and spatial structure, and therefore both its principal components and orientation with respect to some molecular marker are sought for. While it is usually possible to determine the former from frozen solutions, the latter can be obtained only when orientation selective measurements are feasible, although the information obtained is often incomplete. A most common example is orientation selective ENDOR measurements carried out on a sample with an EPR spectrum dominated by an anisotropic g, which provides the orientation of the hyperfine interaction with respect to the g-principal axis system.[1,2] The latter is usually related

to the local symmetry axis, thereby providing structural information. Obviously, single crystal measurements yield the most complete and accurate data, because they provide the complete tensor with respect to the crystallographic axes. Unfortunately, single crystals of proteins are usually very small and consequently make EPR and ENDOR experiments on paramagnetic metal-ion sites at conventional X-band frequency very difficult. This is particularly true for ENDOR measurements for which the S/N requirements are more severe than for EPR. The increased sensitivity of high-field EPR to size-limited samples turns single crystal measurements of metalloenzymes into a viable option, as was shown by the pioneering W-band EPR/ENDOR measurements on the type I Cu(II) in single crystals of azurin.[3,4]

The Mn²⁺ ion is an important ion in enzymes particularly due to its binding to oxygen at active sites.[5,6] It also comprises the active site in oxalate decarboxylase[7] and it can play a structure stabilizing role as found in concanavalin A.[8] In addition, Mn²⁺ has been often used as a substitute for Mg²⁺, which does not have a unique spectroscopic signature.[9] The first EPR study of Mn²⁺ interaction with a protein dates from 1958 by Malmström *et al.* who investigated it with enolase.[10] The EPR spectrum of Mn²⁺, ($S = 5/2$, $I = 5/2$) in the solid state is dominated by the zero-field splitting (ZFS) and the ⁵⁵Mn hyperfine interactions. When the ZFS is large, the X-band spectrum of a frozen solution suffers from severe

broadening due to the ZFS interaction.[11] While the central EPR transitions $\left|-\frac{1}{2}, m_I\right\rangle \leftrightarrow \left|\frac{1}{2}, m_I\right\rangle$ depend on the ZFS parameter, D, to a second order (proportional to D/v_0), the other transitions exhibit a first order dependence on D. Consequently, they often escape detection because of excessive broadening, primarily in continuous wave (CW) EPR. Increasing the magnetic field results in a significant narrowing of the central transitions and therefore Q-band EPR has often been the frequency of choice for Mn²⁺ studies. Orientational information regarding ligand hyperfine interactions usually cannot be obtained from Mn²⁺ in frozen solutions, because the EPR spectrum is dominated by the central transitions that exhibit a low degree of anisotropy. Hence, the orientational information can be derived only from single crystal measurements. The availability of high-field EPR/ENDOR makes such measurements feasible. Since the protein molecules are large, the distance between the Mn²⁺ ions of neighboring molecules is large enough, such that the spin–spin exchange interaction become negligible and the ⁵⁵Mn hyperfine components are well resolved. In contrast, in measurements of single crystals of small molecules, the paramagnetic metal ion has to be doped into a similar diamagnetic host to eliminate the intermolecular spin exchange. The negligible spin–spin interaction also increases the echo decay times, thereby permitting pulsed EPR/ENDOR measurements.

The degree of dynamic and structural information on Mn²⁺ sites in proteins that can be derived from single crystal high field EPR and ENDOR is presented in this overview, emphasizing its complementarity with X-ray crystallography data, namely, focusing on local motions and the location of protons. As a model we have chosen the protein concanavalin A, which has been extensively studied in the past and its 3D structure was determined at an exceptionally high resolution,[12] 0.94 Å. Concanavalin A is a member of the plant haemagglutinin (or plant lectin) family; a large and ubiquitous group of saccharide-binding proteins whose biological function is as yet unknown.[8] The importance of these proteins is expressed in their ability to bind saccharides; each member of the family has a unique saccharide specificity.[8] The overall structure of the stable protein dimer is dominated by an extensive β sheet strand arrangement, the so called *jellyroll motif*. This further associates as a dimer of dimers to form a tetramer of 100 kDa total molecular weight. Each monomer has a molecular weight of 25 kDa comprising 237 amino acids, and containing two metal binding sites, one, called S1, is occupied by a transition-metal ion, e.g. Mn²⁺, and the other, S2, by Ca²⁺, as shown in Fig. 1. Occupancy of both sites is essential for saccharide binding. The Mn²⁺ site has a slightly distorted octahedral geometry in which the Mn²⁺ is coordinated to the carboxyl groups of Asp10, Asp19, Glu8; the imidazole N$_\varepsilon$ of His24; and two water molecules. The carboxyl groups of Asp10 and Asp19 form a bridge to the Ca²⁺. The role of the transition-metal ion in this protein is structural; namely the Mn²⁺, together with the Ca⁺² serve as stabilizers for the loops that constitute the saccharide binding site. The crystal has an orthorhombic symmetry (space group I_{222}), with unit cell parameters $a = 89.2$Å, $b = 87.2$Å, $c = 62.9$Å. The ZFS of

the Mn⁺² ion was determined at room temperature (RT) by single crystal Q-band CW EPR spectroscopy.[13]

Here we shall first present single crystal EPR and field-sweep echo-detected (FS-ED) measurements at RT and low temperatures which were used to determine the Mn²⁺ ZFS tensor and to characterize local motion at the Mn²⁺ site.[14] This was followed by ¹H ENDOR measurements determining the location of the protons of the water and histidine ligands,[15] in an attempt to localize the detected motion. Finally, new ⁵⁵Mn ENDOR results, from which information regarding the nuclear quadrupole interaction and its sensitivity to the motion detected by the EPR measurements, are described.

Brief theoretical background and definitions

The spin Hamiltonian of ⁵⁵Mn²⁺ ($d^5, S = \frac{5}{2}, I = \frac{5}{2}$) coupled to n protons is given by:

$$\mathcal{H} = g\beta B_0 \hat{S}_Z + \hat{S}\cdot\mathbf{D}\cdot\hat{S} + a_{iso}\hat{I}_M\cdot\hat{S}_M - g_M\beta_N B_0 \hat{I}_{MZ} + \hat{I}_M\cdot\mathbf{P}\cdot\hat{I}_M$$
$$+ \sum_{i=1}^{n}(\hat{I}_{Hi}\cdot\mathbf{A}_{Hi}\cdot\hat{S} - g_H\beta_N B_0 \hat{I}_{HiZ}) \qquad (1)$$

In Eqn 1 the first and second terms correspond to the electron Zeeman and the ZFS interactions respectively. The next three terms represent ⁵⁵Mn hyperfine, Zeeman and quadrupole interactions respectively. Finally, all terms under the summation correspond to the ¹H hyperfine and Zeeman interactions respectively. Since $\mathbf{D}$ is traceless, the ZFS term can be expressed with just two parameters as follows:

$$\hat{S}\cdot\mathbf{D}\cdot\hat{S} = \frac{D}{3}[3\hat{S}_z'^2 - S(S+1)] + E(\hat{S}_x'^2 - \hat{S}_y'^2) \qquad (2)$$

where $D = \frac{3}{2}D_{zz}$, $E = (D_{yy} - D_{xx})$ and the coordinates x, y and z refer to the principal axis system of the ZFS tensor. For concanavalin A, $D \ll g\beta B_0$ at W-band and therefore second-order perturbation theory can be used to analyze the spectrum according to the expressions given in the literature.[11,16] When the EPR spectrum is analyzed, only

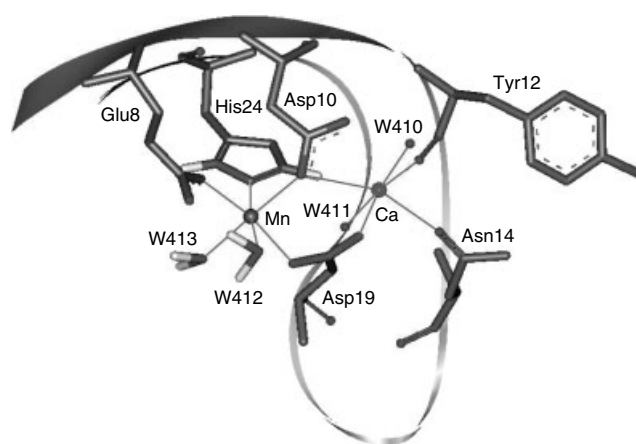**Figure 1.** The binding sites of the Mn²⁺ and Ca²⁺ sites in concanavalin A.[12] The protons were added according to the coordinates determined from ¹H ENDOR measurements. The protein x-ray structure data was taken from the Protein Data Bank (1nls).

the first three terms in Eqn 1 should be considered. When the proton ENDOR is of interest, the ZFS and ^{55}Mn interaction do not affect the ENDOR frequencies.[15] Hence, they can be well described by the first order expression given for each proton by:[17]

$$\nu_{M_S}(H) = M_S[T_\perp(3\cos^2\theta - 1) + a_{iso}] - \nu_I \quad (3)$$

where ν_I is the Larmor frequency, a_{iso} is the isotropic hyperfine constant and θ is the angle between the direction of the unique axis of the hyperfine interaction and the external magnetic field, $\vec{B}$. Equation 3 is valid for an axially symmetric hyperfine interaction and when the point-dipole approximation applies, $T_\perp$ is related to the electron–nuclear distance r according to:

$$T_\perp = \frac{\mu_0}{4\pi h}\frac{(gg_N\beta\beta_N)}{r^3}, \quad (4)$$

and the unique axis of the interaction is along $\vec{r}$.

We have shown that the ENDOR frequencies of an electron high spin system may be affected by the ZFS and thereby show orientation dependence although its hyperfine interaction is isotropic.[18] This occurs when both the ZFS and the hyperfine couplings are substantial compared to the electron spin Zeeman interaction and the effect is of the order of $\frac{a_{iso}D^2}{\nu_0^2}$.[18] At high enough fields, this dependence is eliminated, as was shown for high spin ^{57}Fe(III) in zeolites.[19] The D value of concanavalin A is relatively small[14] Carmieli03 and therefore at 95 GHz, its contribution is of the order of tens of kHz and can be neglected. Hence, to second order of the isotropic hyperfine interaction and first order of the nuclear quadrupole interaction, the ENDOR frequencies within a particular M_S manifolds are given by:[18,20,21]

$$\nu_{M_S}(Mn) = M_S a_{iso} - \nu_I + P(2m_I - 1)$$
$$+ \frac{a_{iso}^2}{\nu_0}[-S(S+1) + (M_S)^2 - M_S(2m_I - 1)] \quad (5)$$

In Eqn 5 $P = \frac{3e^2qQ}{8I(2I-1)h}[(3\cos^2\theta' - 1) + \eta\sin^2\theta'\cos(2\phi')]$ and $\eta = \frac{P_{xx} - P_{yy}}{P_{zz}}$ is the asymmetry parameter, θ and ϕ are the orientation of the principal axis system of the quadrupole tensor with respect to the magnetic field and ν_0 is the electron spin Larmor frequency. It is convenient to consider the sum and differences of the measured ENDOR frequencies of the same m_I value within the $M_S = \pm\frac{1}{2}$ manifolds,[20] which yield for the strong-coupling case, $|\frac{1}{2}a_{iso} - \nu_I| > 0$:

$$\Delta\nu_{\pm\frac{1}{2}} = 2\nu_I - 2P(2m_I - 1) + \frac{17}{2}\frac{a_{iso}^2}{\nu_0} \quad (6)$$

$$\bar{\nu}_{\pm\frac{1}{2}} = a_{iso} - \frac{a_{iso}^2}{\nu_0}(2m_I - 1) \quad (7)$$

A detailed analysis of the ^{55}Mn ENDOR spectra, not including ZFS and nuclear quadrupole effects, has been given by Britt and coworkers.[20] The inclusion of the nuclear quadrupole interaction has been considered in the case of ^{51}V.[21]

In the single crystal measurements, we used the following reference frames: the principal axis system of the magnetic tensor, $M(x, y, z)$, the crystal frame $C(c, b, a)$, the sample tube frame $T(x', y', z')$, where z' is parallel to the tube axis, the goniometer frame $G(x'', y'', z'')$ and the lab frame $B(X, Y, Z)$, where $Z \parallel \vec{B}$. The transformation between these axis systems is done using the appropriate Euler angles and the tensor transformations are carried out using the corresponding Wigner rotation matrices, $R(\alpha', \beta', \gamma')$. For our experimental set up the transformations are:

$$M \xrightarrow{\alpha, \beta, \gamma} C \xrightarrow{\phi', \theta', \psi} T \xrightarrow{0, 0, \phi_0} G \xrightarrow{\phi_r, 90, 0} B \quad (8)$$

The rotation patterns are acquired by measuring the spectrum as a function of the rotation angle of the goniometer, ϕ_r. The relation between the above sets of angles and the angles θ and ϕ used in Eqns 3,5 and in the expressions used in the EPR simulations[11,13] is:

$$R(0, \theta, \phi) = R(\alpha, \beta, \gamma)R(\phi', \theta', \psi)R(0, 0, \phi_0)R(\phi_r, 90, 0) \quad (9)$$

All angles in Eqn 9, besides α, β and γ, are defined by the experimental conditions. There are four Mn^{2+} centers per unit cell in the crystals of concanavalin A[12] and, according to the I_{222} space group, their α, β and γ are related as described in Table 1.

Conformational dynamics at the Mn^{2+}

The RT single crystal Q-band spectra, reported by Meirovitch et al.[13] were fully consistent with the crystal symmetry and the X-ray determined structure, where there is one tetramer in the asymmetric unit with one type of Mn^{2+} per monomer. Accordingly, when the crystal is oriented with the magnetic field parallel to any of the crystallographic axes, all four Mn^{2+} are equivalent, whereas for any orientation within any of the crystallographic planes, two pairs of the four crystallographic sites can be resolved. Room-temperature, W-band measurements[14] were consistent with the Q-band results, and analysis of the CW EPR rotation patterns just refined the previously determined ZFS tensor.[13] In contrast, rotation patterns recorded at low temperatures did not agree with the above, and two chemically inequivalent Mn^{2+} were clearly resolved. A comparison of the W-band CW EPR rotation patterns of the ac plane acquired at RT and at 4.5 K is presented in Fig. 2. The two ZFS tensors determined from these measurements at both temperatures[14] are given in Table 2. These show that the differences in the D and E values of the two Mn^{2+} types are significant. The rotation patterns also show that each type consists of four crystallographic sites, which are related by the I_{222} symmetry of the crystal.

Table 1. The Euler angles relating the principal axis system of the magnetic tensors with the crystallographic axis system for the four Mn^{2+} sites of concanavalin A

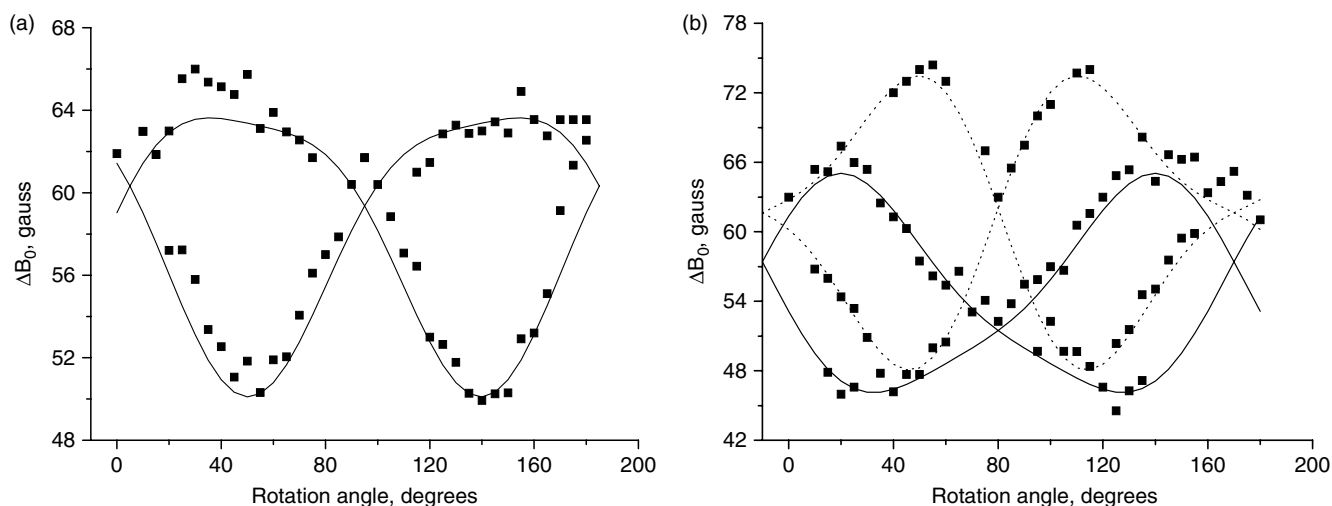|	α	β	γ
Site I	α	β	γ
Site II	α	β	$\gamma + 180$
Site III	$180 + \alpha$	$180 - \beta$	$180 - \gamma$
Site IV	$180 + \alpha$	$180 - \beta$	$-\gamma$

Figure 2. W-band CW EPR rotation pattern of the *ac* plane of the highest field ^{55}Mn hyperfine component of a single crystal of concanavalin A measured at (a) RT (b) 4.5 K. The resonant magnetic field, ΔB_0 is given with respect to 3.4 T. The lines are simulations obtained with the parameters listed in Table 1, where in (b) the solid line corresponds to Mn_A^{2+} and the dashed line to Mn_B^{2+}. Reproduced from Ref. 14.
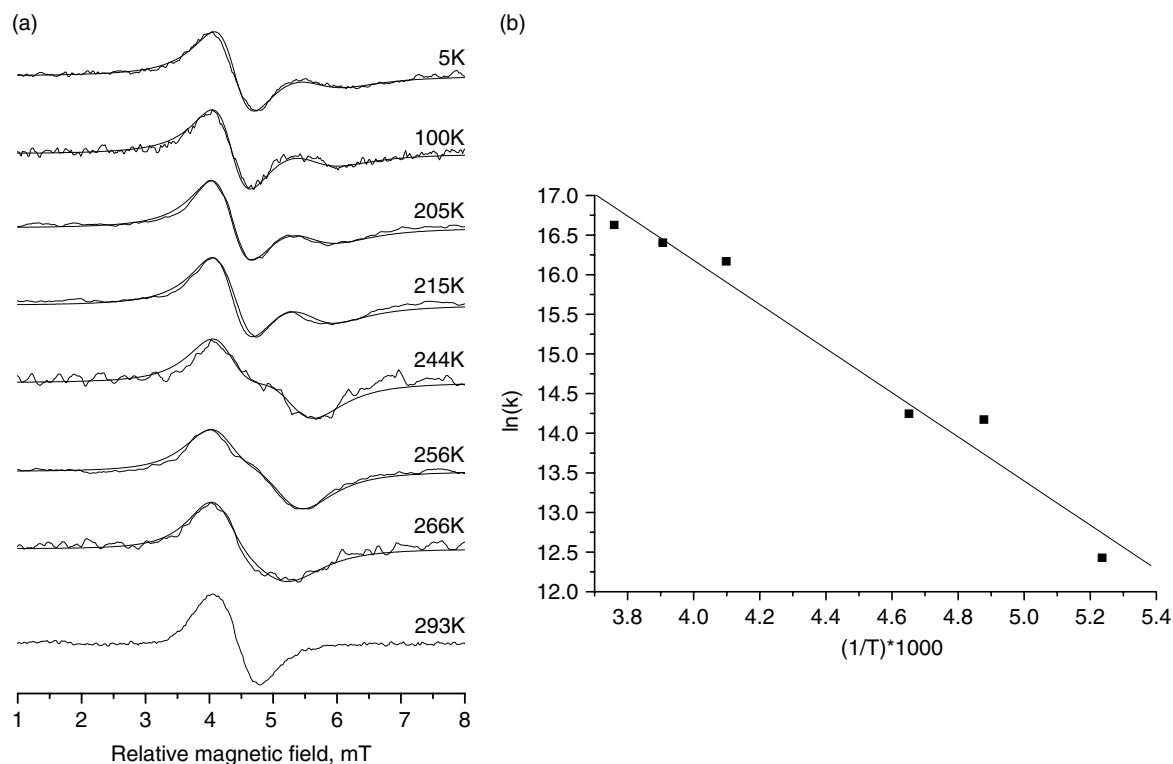

Figure 3. (a) The temperature dependence of the CW EPR spectra of a single crystal of concanavalin A oriented with $\vec{B} \parallel a$ and simulations obtained with the parameters given in Table 3. Only the region of the highest field ^{55}Mn hyperfine components is displayed. (b) The temperature dependence of k as determined from the simulation shown in (a). Reproduced from Ref. 14.

These results, however, are inconsistent with the high-resolution X-ray crystallography structure, determined also at a low temperature (110 K) where only one Mn^{2+} site has been identified.[12] Two possible models are consistent with the EPR results; in the first there are two types of tetramers, randomly distributed in the crystal, and in each one all the Mn^{2+} are equivalent. Alternatively, each tetramer contains a random distribution of the two inequivalent Mn^{2+}.

To rationalize the temperature effect on the Mn^{2+} site, the magnetic field was set parallel to the *a* axis, where the two sextets are resolved, and the EPR spectrum was measured as a function of temperature,[14] as shown in Fig. 3a. Here, only the highest field ^{55}Mn hyperfine component of the sextet is depicted and an arbitrary relative field is used for the abscissa to avoid using large numbers. In this experiment, the RT spectrum was first recorded, the crystal

Table 2. Summary of the ZFS parameters at room temperature and at 4.5 K. In all cases the ^{55}Mn hyperfine coupling was 265 MHz. The angles are with respect to the (c,b,a) crystal system (^{a} The angles in the original paper are given with respect to the (c,a,b) crystal system[14])

Mn sites	$D(\pm 10)^a$ MHz	$\frac{E}{D}(\pm 0.005)$	$\alpha \pm 5$ (degrees)	$\beta \pm 3$ (degrees)	$\gamma \pm 5$ (degrees)
Mn^{2+} (RT)	726	0.115	34	127	41
$Mn_A{}^{2+}$ (4.5 K)	789	0.24	59	118	44
$Mn_B{}^{2+}$ (4.5 K)	970	0.145	2	135	52

was then rapidly cooled to 4.5 K and then measurements were performed by increasing the temperature. It was not possible to cool the crystal slowly past the freezing point because it broke. Furthermore, during the heating process (from 4.5 K and up) it was not possible to reach RT because the crystal got damaged upon thawing. Because of these limitations, measurements in the region of 273 K were not performed. The spectra in Fig. 3a show that up to 205 K the spectrum is invariant and can be simulated as a superposition of two Lorentzian lines with different widths and relative intensities. Above 205 K the separation between the lines decreases significantly, until they merge into a single line at RT. These lineshape changes are typical of a dynamic process involving a two-site exchange. The spectra were simulated[14] using the following simple process:

$$Mn_A{}^{2+} \underset{\tau_b^{-1}}{\overset{\tau_a^{-1}}{\rightleftarrows}} Mn_B{}^{2+} \qquad (10)$$
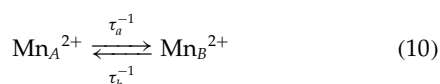
employing the standard expressions.[22] Here τ_a and τ_b are the appropriate rate constants, whereas the relative populations of $Mn_A{}^{2+}$ and $Mn_B{}^{2+}$ are given by f_a and f_b, $(f_a + f_b) = 1$. The difference in the resonant field positions is ΔB and $\frac{1}{\tau} = \frac{1}{\tau_a} + \frac{1}{\tau_b} = k$. The simulated traces are depicted in Fig. 3a and they show that the rate constant increases with temperature and at 266 K it reaches $6 \cdot 10^8$ s^{-1}. The two states are not equally populated, at low temperatures $f_a = 64\%$, whereas, at 266 K it decreases to 38%. In addition, the linewidths of both decrease with temperature, with the width of $Mn_A{}^{2+}$ being consistently lower than that of $Mn_B{}^{2+}$. An Arrhenius plot of the temperature dependence of k, presented in Fig. 3b, gave an activation energy of 23.8 kJ/mol and $\Delta S_e = 3.2$ kJ/mol for the entropy activation.[14]

This two-site exchange model further implies that the ZFS tensor in the fast motion regime, i.e. at RT should be a weighted average of the two low-temperature tensors. Indeed, the Euler angles and the E values of the average tensor are close to those of the RT tensor.[14] The experimental D value, however, was found to be lower than the value of each of the low temperature sites and differed significantly from the averaged value. This was attributed to an additional local motion that leads to the reduction of D. This is consistent with the observed temperature dependence of the linewidth of both $Mn_A{}^{2+}$ and $Mn_B{}^{2+}$, which suggests the existence of a distribution within each state, namely, the minima are rather broad with that of $Mn_B{}^{2+}$ being broader. As the temperature increases, the width of this distribution decreases because of motional averaging and this is accompanied by a reduction in D. The EPR results also

show that the ^{55}Mn hyperfine coupling, $|a_{iso}| = 265$ MHz, was the same for $Mn_A{}^{2+}$ and $Mn_B{}^{2+}$, showing that it is less sensitive to the local environment as compared to the ZFS.

The question that arises is what is the motion that leads to the modulation of the ZFS tensor? It can be a low amplitude motion of the Mn^{2+} ion itself, the motion of one (or more) of the ligands or even some motion of larger subunits that affects the coordination sphere of the Mn^{2+} ion. Molecular tumbling is ruled out, because the protein is in a crystalline state. Further insight into identification of the specific local motion in terms of the residues involved, can, in principle, be obtained from ENDOR measurements which probe the ligands. Such experiments are described next.

^{1}H ENDOR measurements

The 3D structure presented in Fig. 1 shows that the histidine and water protons are the closest to the Mn^{2+} ions and therefore they dominate the ^{1}H ENDOR spectrum. ^{1}H ENDOR rotation patterns were collected for both ab and ac planes at the magnetic field corresponding the highest field ^{55}Mn hyperfine component.[12] This EPR line is often split because of the presence of distinct Mn^{2+} sites and the ENDOR spectra were recorded for each resolved feature. The signals of the water and the imidazole ring protons were assigned by comparing the ^{1}H ENDOR spectra of crystals grown in H_2O and D_2O, where the water signals are absent from the spectra of D_2O crystals. The signs of the hyperfine splittings were determined through assignment of the ENDOR signals to their respective $M_S = \pm\frac{1}{2}$ manifolds. This was achieved by recording the ENDOR spectra at magnetic field positions where the contributions of the $\left|-\frac{1}{2}, m_I\right\rangle \longrightarrow \left|\frac{1}{2}, m_I\right\rangle$ transitions are negligible and those of the $\left|-\frac{3}{2}, m_I\right\rangle \longrightarrow \left|-\frac{1}{2}, m_I\right\rangle$ are substantial.[23] Under such conditions the contribution of the $M_S = \frac{1}{2}$ ENDOR line is considerably diminished.

We first focus on the ENDOR spectra for a crystal orientation a $\parallel \vec{B}$ where the RT EPR spectrum shows one signal, but at low temperature, spectrum $Mn_A{}^{2+}$ and $Mn_B{}^{2+}$ are resolved (see inset in Fig. 4). The ENDOR spectra shown in Fig. 4, recorded at field positions (a) and (b), corresponding to $Mn_A{}^{2+}$ and $Mn_B{}^{2+}$, respectively, are the same, suggesting that the arrangement of protons with respect to the Mn^{2+} is identical for both types. Note the appearance of signals arising from the $M_s = -\frac{3}{2}$ manifold, which do not have a symmetric counterpart with respect to ν_I. The relative intensities of the signal are somewhat larger when recorded at field position (b) due to the larger contribution of the $\left|-\frac{3}{2}, m_I\right\rangle \longrightarrow \left|-\frac{1}{2}, m_I\right\rangle$ transition at this field. This similar behavior of the two types was further confirmed in the
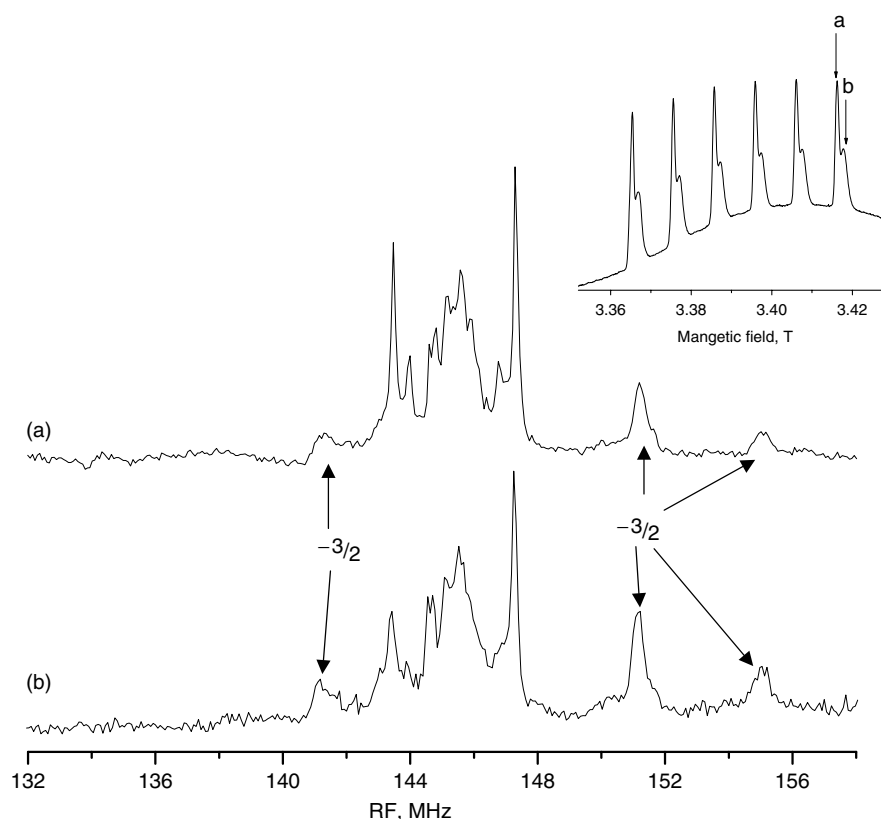
Figure 4. ^{1}H Davies ENDOR spectra recorded for a crystal orientation of $\vec{B} \parallel a$ and the field set to positions a and b as indicated in the inset. The inset shows the corresponding FS-ED EPR spectrum at 4.5 K. Experimental conditions are as described in Ref. 15 Signals arising from the M$_S = -\frac{3}{2}$ manifolds are noted.

complete rotation patterns. The ^{1}H ENDOR ab rotation pattern of the imidazole protons[15] is depicted in Fig. 5. It shows the presence of two chemically inequivalent protons, corresponding to the two imidazole protons (see Fig. 1). For each, signals of two pairs of crystallographic sites can be resolved, which merge into one at the crystallographic axes, as expected for a I_{222} symmetry and one Mn^{2+} type. The same behavior was observed for the ac plane. This indicates that the orientation and distance of the imidazole protons with respect to the Mn^{2+} is the same for Mn$_A^{2+}$ and Mn$_B^{2+}$.

The hyperfine tensor parameters of the two imidazole protons obtained from the fit of the rotation patterns are listed in Table 3, where the Mn–H distance has been derived from $T_\perp$ using the point-dipole approximation (see Eqn 4).[15] From the rotation patterns, four different sets of parameters were obtained for each proton. Those belonging to one molecule

were identified by taking into account the imidazole group geometry, namely, H–H distances were calculated from the Mn–H distances and orientations. On the basis of the proton coordinates obtained, and using the X-ray determined coordinates of the imidazole group,[12] H_{im1} was assigned to H_δ and H_{im2} to H_ε (see Fig. 1).[15] The protons positions determined from the ENDOR measurements are in very good agreement with the 3D structure in which the protons were added using the molecular modeling software Insight II.[15]

Once the signals of the imidazole protons were assigned, it was possible to extract the water protons rotation patterns and analyze them.[15] Their behavior was similar to that of the imidazole protons, namely, the spectra of Mn$_A^{2+}$ and Mn$_B^{2+}$ were identical. Four different protons were identified and the rotation patterns of H$_{w1}$ and H$_{w2}$ are presented in Figs. 6. Each of these rotation patterns show that two pair of

Table 3. Summary of the hyperfine coupling parameters of the imidazole and water protons. The angles are with respect to the (c,b,a) crystal system[14]

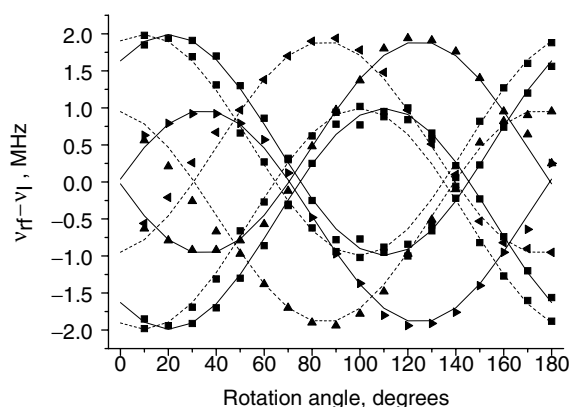| Proton	$T_\perp (\pm 0.04)$ MHz	$a_{iso}(\pm 0.04)$ MHz	$\beta \pm 0.5$ (degrees)	$\gamma \pm 0.5$ (degrees)	$r_{Mn-H} \pm 0.02$ Å
H$_{im1}$	1.94	0.08	83	−70.3	3.44
H$_{im2}$	1.99	0.08	89.5	5.3	3.41
H$_{w1}$	3.49	0.8	78.3	143.0	2.82
H$_{w2}$	3.96	0.1	112.9	134.0	2.71
H$_{w3}$	2.5	0.4	47.0	50.0	3.16
H$_{w4}$	3.9	0.4	67.0	72.0	2.72

Figure 5. The ^{1}H ENDOR rotation patterns of the imidazole protons in the *ab* plane. The square and the triangles indicate H$_{im2}$ and H$_{im1}$, respectively, and the dotted and solid lines indicate site I and site II, respectively. Reproduced from Ref. 15.

one Mn^{2+} center, where H$_{w1}$ and H$_{w2}$ belong to one water molecule and H$_{w3}$ and H$_{w4}$ to the second water molecule.[15] The parameters of the other three centers can be obtained by the relations given in Table 1.

The assignment of the protons to the two different water oxygens, O$_{412}$ and O$_{413}$, of the crystal structure was done by calculation of the O–H distance using the X-ray-[12] and ENDOR determined coordinates. This gave reasonable O$_{412}$–H$_{w1}$ and O$_{412}$–H$_{w2}$ distances of 1.16 and 0.97Å respectively, and an HO$_{412}$H angle of 104.6°. The calculated HO$_{413}$H angle, however, was 86°, which is too small. Nevertheless, if O$_{413}$ is displaced 0.05 Å away from the Mn^{2+} ion, the angle increases to 102.3°. An error of 0.05 Å in the oxygen position cannot be excluded considering the X-ray diffraction resolution. On the basis of the ENDOR results, the protons were placed on the XRD 3D structure shown in Fig. 1. These results show that both water ligands are ordered in the crystal, at least at low temperatures. Moreover, they are involved in hydrogen bonds, showing that besides acting as ligands, they have a role in stabilizing the tertiary structure of the protein. H$_{w1}$ and H$_{w2}$ are hydrogen bonded to Val32 and Glu8, whereas, H$_{w3}$ and H$_{w4}$ are close to the oxygen (O$_\gamma$) of the hydroxyl group of Ser34.[15]

To summarize, the ^{1}H ENDOR measurements allowed to determine the coordinates of the water protons and to identify the H-bonds they are involved in. The information regarding the location of water protons cannot be obtained
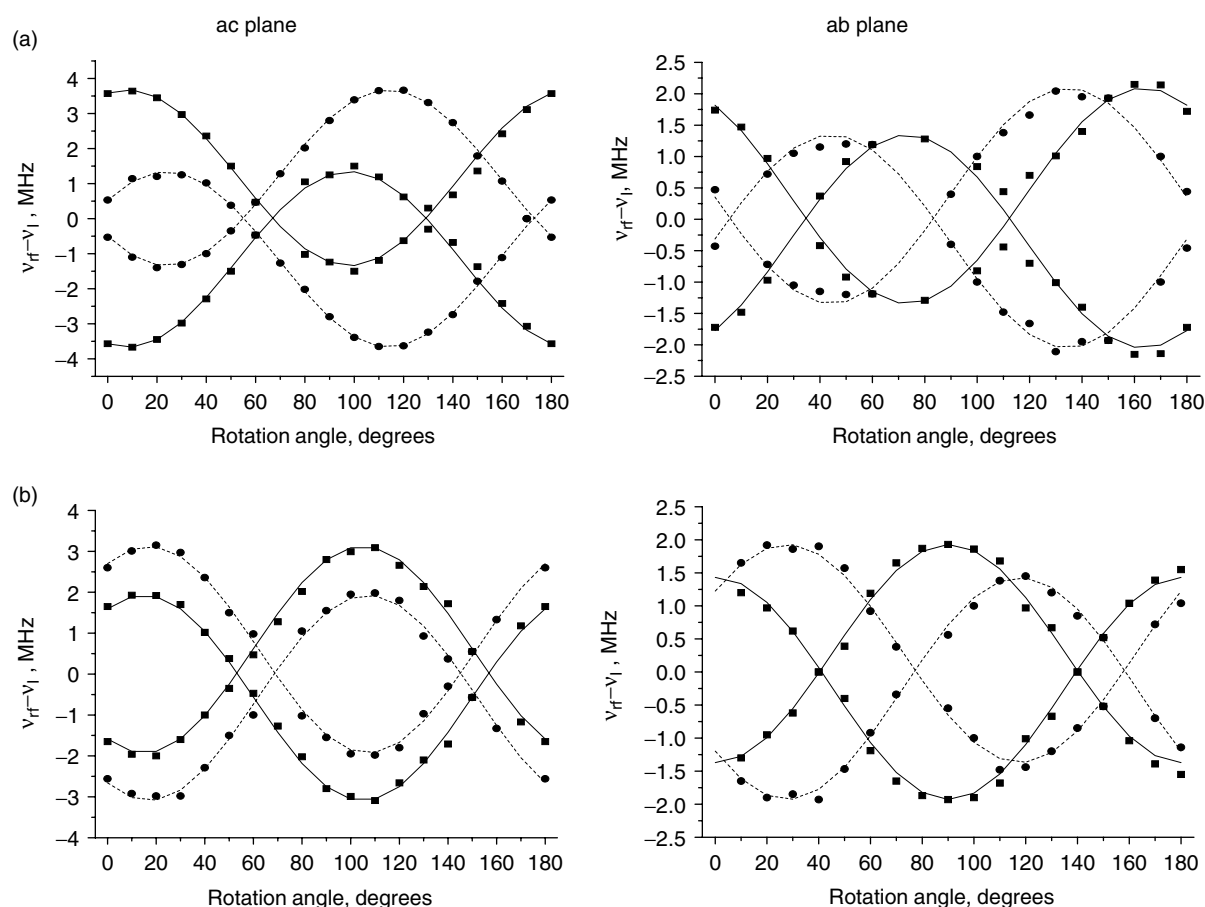
sites are resolved in each crystallographic plane. The best-fit simulated rotation patterns for each proton are presented as solid lines and dashed lines in Fig. 6 and $a_{iso}, T_\perp, r, \beta$ and γ obtained are listed in Table 3. Again, the protons belonging to one molecule were identified as described for the imidazole protons by calculating H–H distances. All the parameters listed in Table 3 are consistent with all protons belonging to

Figure 6. The ^{1}H ENDOR rotation patterns of the (a) H$_{w1}$ and (b) H$_{w2}$ water protons in the *ac* and *ab* plane. The squares and the circles indicate site I and site II, respectively. Reproduced from Ref. 15.

from the crystallography data. Interestingly, neutron diffraction measurements carried out on concanavalin A, aimed at the determination of the position of the water protons, detected only three protons.[24] It has also been shown that the water and imidazole protons are not sensitive to the differences between the Mn_A^{2+} and Mn_B^{2+}, namely, their Mn–H distance and orientation are the same for the two types, and therefore we conclude that they are not involved in the local motion. This suggests that it is one (or more) of the carboxylates ligands that are involved in the dynamics.
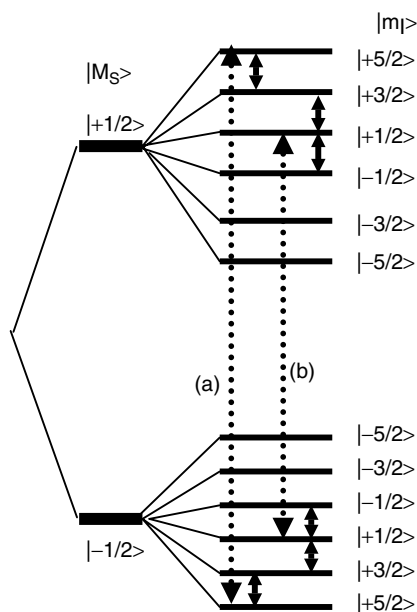

Figure 7. A schematic energy level diagram of the $M_S = \pm\frac{1}{2}$ manifolds showing EPR transitions, dashed lines (a) and (b), along with the corresponding allowed ENDOR transitions (solid lines).

⁵⁵Mn ENDOR measurements

Another indication for the source of the difference between Mn_A^{2+} and Mn_B^{2+} can, in principle, be derived from ⁵⁵Mn ENDOR, which provides the ⁵⁵Mn hyperfine and nuclear quadrupole interactions. While the former has already been determined by the EPR measurements and was found to be insensitive to the difference between the two types, the latter maybe a better probe. Recently, we have characterized the Mn(II) coordination environment in a number of MnAlPO$_n$ materials by W-band ⁵⁵Mn ENDOR.[25] There, several Mn(II) types were distinguished by their different hyperfine couplings, but the quadrupole interaction was not resolved. The measurements, however, were carried out on polycrystalline samples exhibiting very broad lines. A recent report on pulsed ENDOR at 275 GHz on a single crystal of 0.2% Mn²⁺ in ZnGeP₂ has shown that the quadrupole coupling can indeed be resolved.[26]

Figure 7 shows the energy levels of Mn²⁺ corresponding only to the $M_S = \pm\frac{1}{2}$ manifolds. Selecting the EPR $\left|-\frac{1}{2}, \frac{5}{2}\right\rangle \rightarrow \left|\frac{1}{2}, \frac{5}{2}\right\rangle$ transition in an ENDOR measurement, noted as (a) Fig. 7, will result in the observation of the $\left|\frac{5}{2}\right\rangle \leftrightarrow \left|\frac{3}{2}\right\rangle$ ENDOR transitions within the two manifolds. Similarly, excitation of the $\left|-\frac{1}{2}, -\frac{5}{2}\right\rangle \rightarrow \left|\frac{1}{2}, -\frac{5}{2}\right\rangle$ EPR transition leads to the observation of only one ENDOR transition in each manifold, the $\left|-\frac{5}{2}\right\rangle \leftrightarrow \left|-\frac{3}{2}\right\rangle$. Selection of any other ⁵⁵Mn hyperfine component in the ENDOR experiment, as e.g. transition (b) in Fig. 7, leads to the observation of two ENDOR lines within each manifold. This behavior is clear in Figure 8b, which presents the FS-ED EPR spectrum recorded for a crystal orientation of $c \parallel \vec{B}$ and the corresponding ENDOR spectra. In this crystal orientation the signals of Mn_A^{2+} and Mn_B^{2+} practically coincide (see Fig. 2b). In a recent study we have determined experimentally the sign of a_{iso} to be negative,[25] which has been further confirmed by 275 GHz ENDOR measurements[26] and therefore the lines corresponding to specific M_S and m_I values can be assigned, as noted on Fig. 8.
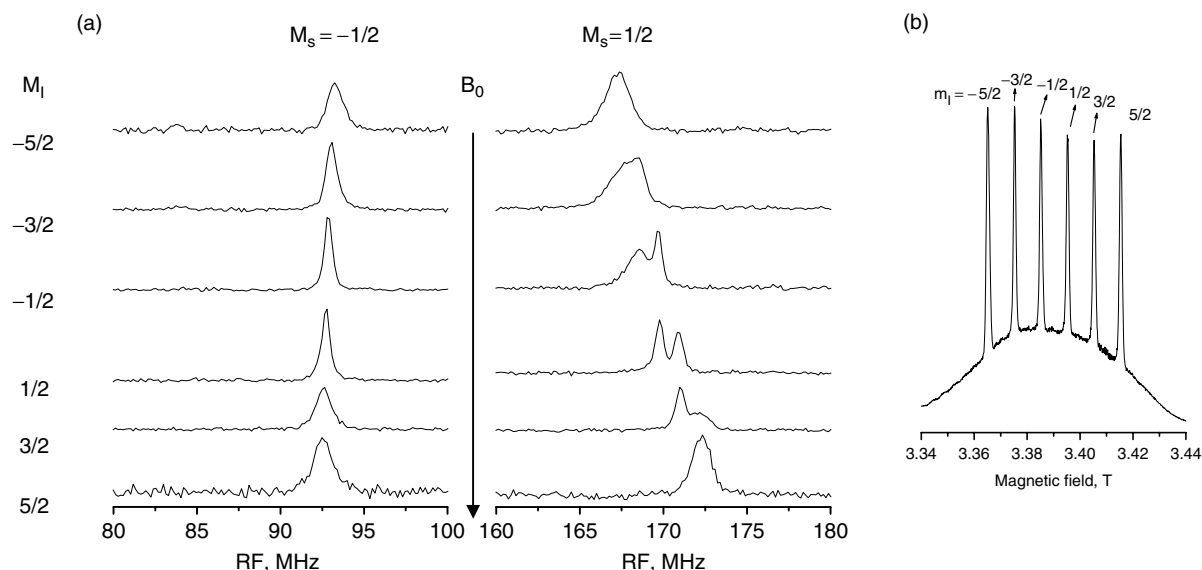

Figure 8. (a) ⁵⁵Mn Davies ENDOR measured at each of the six ⁵⁵Mn hyperfine components in the spectral regions of the $M_S = \pm\frac{1}{2}$ manifolds for a crystal orientation $\vec{B} \parallel c$. (b) corresponding FS-ED EPR spectrum. The experimental conditions: microwave pulse lengths were 0.12, 0.06, 0.12 μs, τ was set to 0.3 μs, and the RF pulse to 5 μs, $T = 6$ K.

Table 4. The ^{55}Mn ENDOR frequencies of the various $m_I \leftrightarrow m_I - 1$ transitions for $M_S = \pm \frac{1}{2}$ manifolds recorded for $\vec{B} \parallel c$ and the P values extracted from them

m_I	$\nu_{+\frac{1}{2}}$, MHz	$\nu_{-\frac{1}{2}}$, MHz	$\bar{\nu}$, MHz	$\Delta\nu - 2\nu_I$, MHz	ν_I, MHz	$\bar{\nu}_{calc}$, MHz	$2P(c)$, MHz
5/2	172.3	92.6	264.9	7.8	35.96	265.5	1.14
3/2	171.0	92.7	263.7	6.6	35.84	263.9	1.13
1/2	169.8	92.8	262.5	5.5	35.74	262.5	1.10
−1/2	168.5	92.8	261.4	4.4	35.65	261.1	1.1
−3/2	167.5	93.1	260.4	3.3	35.55	259.5	

The ^{55}Mn ENDOR spectra recorded at each of the m_I components is given in Figure 8a and the ENDOR frequencies are listed in Table 4. The spectra corresponding to the $M_S = \frac{1}{2}$ manifold are well resolved. As expected, selection of the $\left| -\frac{1}{2}, \pm\frac{5}{2} \right\rangle \leftrightarrow \left| \frac{1}{2}, \pm\frac{5}{2} \right\rangle$ transitions produce only one line while for the others, two resolved line are present,[20] the splitting of which is given to first order by $2P$ (see Eqn 5). Interestingly, the linewidth increases with the m_I value. This is attributed to the quadrupolar interaction that scales with the m_I value, and therefore slight misalignment and differences between the two Mn^{2+} types will be enhanced for higher m_I values. In contrast to the $M_S = \frac{1}{2}$, the $M_S = -\frac{1}{2}$ does not resolve the quadrupolar splittings and the shifts of the frequencies of different m_I components are significantly smaller. This resolution difference becomes understandable when second order (see Eqn 5) contributions due to the hyperfine coupling are taken into account. For one manifold, it has the same sign as the quadrupolar term, whereas, for the other it has the opposite sign. These effects are also manifested in the m_I dependence of $\bar{\nu}$ (see Table 4). This shows that the first order approximation for the ^{55}Mn hyperfine interaction is not valid, even at W-band.

From Eqn 7 it is clear that a_{iso} should be determined from the $m_I = -\frac{1}{2}$ component, thus refining the −265 MHz value obtained from the EPR spectra to −262.5 MHz. The calculated $\bar{\nu}$ values obtained with this a_{iso} value (Eqn 7) are listed in Table 4, showing that a discrepancy of about 0.5 MHz still exists. This can be attributed to second-order terms of the quadrupole interaction or third-order terms of the hyperfine interaction. The value of P at this crystal orientation, denoted by $P(c)$ is 0.55 ± 0.02 MHz.

The ^{55}Mn ENDOR spectra measured at the $c \parallel \vec{B}$ orientation are consistent with the low-temperature EPR results which do not resolve Mn_A^{2+} and Mn_B^{2+} at this orientation, and only one quadrupolar splitting was obtained. Measurements carried out at $a \parallel \vec{B}$ where the two types are well resolved are shown in Fig. 9. The spectra were measured with the field set to the lowest field ^{55}Mn hyperfine component, $m_I = -\frac{5}{2}$. The top traces were measured at position a, corresponding to Mn_A^{2+} while the bottom spectra, recorded at position b, correspond to Mn_B^{2+}. The spectra reveal significant shifts, indicating that at this orientation quadrupole interaction of the two Mn^{2+} types are different. Using Eqn 6 we obtained for Mn_A^{2+} $P(a) = 0.57$ MHz, whereas for Mn_B^{2+} $P(a) = 0.26$ MHz. A full analysis of the ^{55}Mn ENDOR determining the two complete quadrupolar tensors is currently underway and will be published elsewhere. Nonetheless, these results show that unlike the ^{1}H
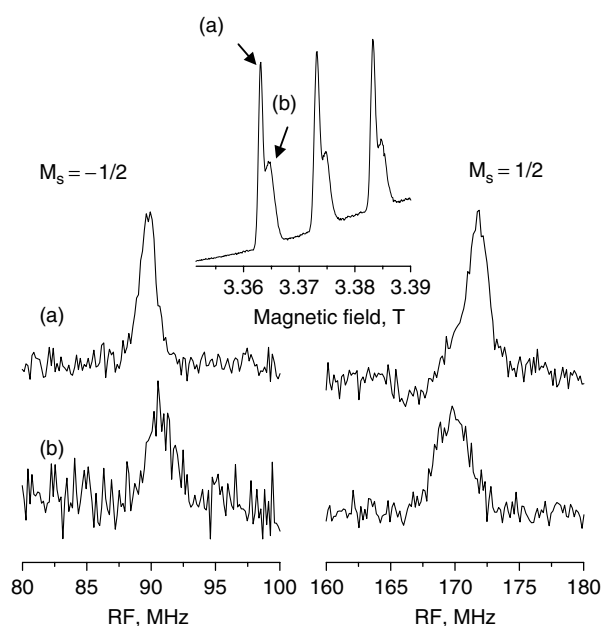
Figure 9. ^{55}Mn Davies ENDOR measured at the lowest field ^{55}Mn hyperfine component in the spectral regions of the $M_S = \pm\frac{1}{2}$ manifolds for a crystal orientation $\vec{B} \parallel a$. The inset shows part of the corresponding FS-ED EPR spectrum and the field positions where measurements took place. The experimental conditions are as in Fig. 8.

hyperfine the ^{55}Mn quadrupole interaction is sensitive to the differences between the two types of Mn. This is actually expected, because this interaction is determined on the electric field gradient at the Mn^{2+} nucleus and should therefore show similar behavior as the ZFS. A remaining question, however, is which one is more sensitive and will they have the same orientation.

DISCUSSION

EPR measurements carried out at a high field on single crystals of concanavalin A yielded highly resolved spectra, free of forbidden transitions, and consequently resolved two chemically inequivalent Mn^{2+} sites, which were not detected by high resolution X-ray diffraction measurements, also carried out at low temperature.[12] Further temperature-dependent measurements revealed a two-site exchange process at the Mn^{2+} site. To the best of our knowledge, this is the first report of a motion at a metal site in a protein crystal.[14] This motion can be associated with a movement of the Mn^{2+} ion or with a motion of one (or more) of its
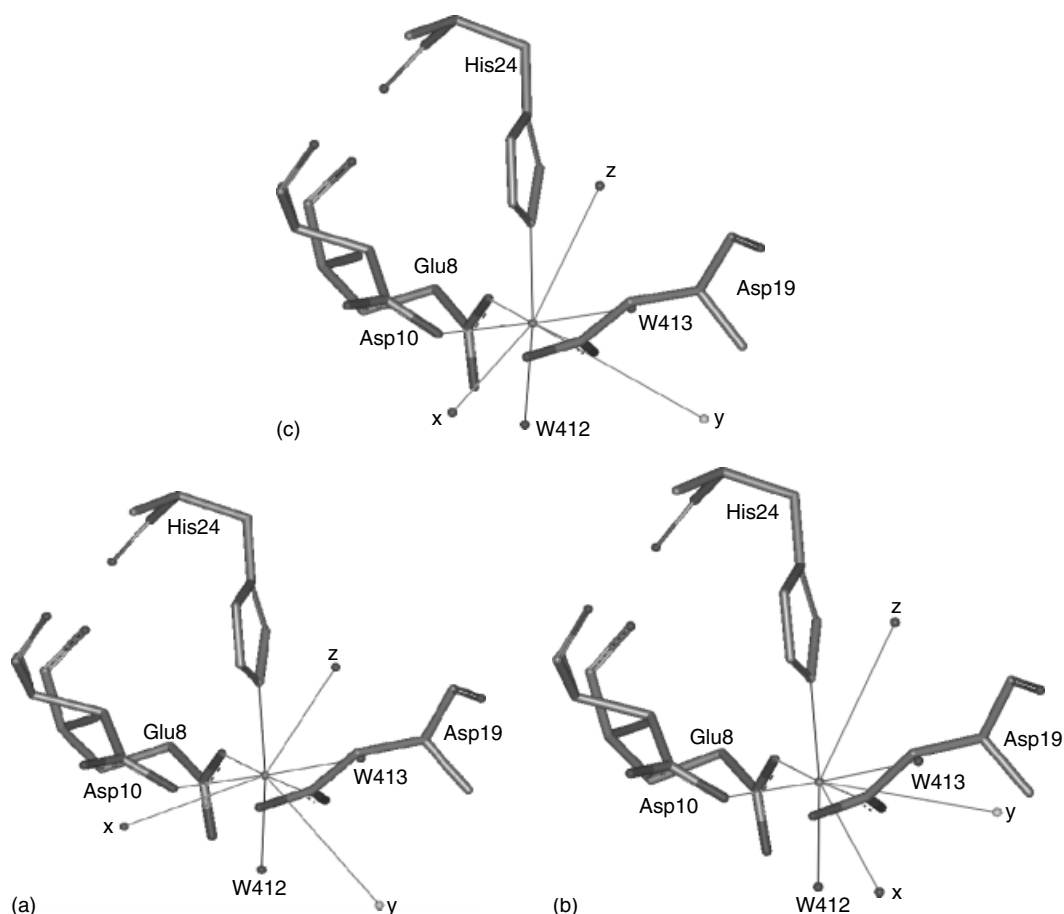
Figure 10. The orientation of the ZFS tensor superimposed on the 3D structure of (A) Mn_A^{2+} at 4.5 K, (B) Mn_B^{2+} at 4.5 K, (C) Mn^{2+} at room temperature. Reproduced from Ref. 14.

ligands. Both possibilities would affect the ZFS and the [55]Mn quadrupole interaction. The observation that the ^{1}H ENDOR spectra of Mn_A^{2+} and Mn_B^{2+} are the same rules out the first possibility. Moreover, it indicates that neither the water molecules, which seem to be the most natural candidate for the motion, nor the imidazole ligand are involved.

In an attempt to identify specific residues in the Mn²⁺ site that are involved in the dynamic process, the orientation of the principal axis systems of the ZFS tensors at RT and low temperature with respect to the available 3D structure were compared.[14] Because of the symmetry of the crystal there are four possibilities to overlay the ZFS frames on the structure and we chose the one where the principal axes were the closest to some local symmetry axis or bond directions. The low-temperature high-resolution 3D structure[12] shows that the Mn²⁺–N and Mn²⁺–O412 distances (the water molecule opposite the nitrogen) are slightly longer (2.233, and 2.261 Å) than the other Mn–O distances, which suggests that z may be along this direction. Indeed, Fig. 10 shows that for one of the options, the z axes of the ZFS of Mn_A^{2+}, Mn_B^{2+} and the RT Mn²⁺ are close to the Mn–N direction (28–38°), while the x and y axes are close to the equatorial plane of the three carboxylate ligands and one water molecule. The orientation of z in all these is similar and the differences between the sites can be practically expressed by a rotation about z. Furthermore, the orientation of the ZFS at RT, Fig. 10C, is the

average of the two low-temperature orientations. The change in orientation is associated with a significant change in E/D from 0.24 to 0.145. It is therefore suggested that the motion is associated with Asp10 and/or Asp19 which are bridging ligands to the Ca²⁺ in the S2 site.[14] This can be verified by ENDOR measurements on concanavalin A with ^{13}C labeled Asp10 or Asp19.

We hope that the complete analysis of the [55]Mn quadrupole tensors of the two sites, will allow to further pinpoint the nature of the dynamic process observed. We also note that the observed dynamics is not a consequence of the freezing, since it has not been observed in similar investigations currently underway on single crystals of Mn²⁺ containing enolase bound to an inhibitor. The described investigations clearly demonstrates the wealth of information that can be obtained by high-field EPR/ENDOR measurements on metalloprotein single crystals. In a frozen solution, it was not possible to resolve the two sites, since their subtle differences were within the linewidth.

Acknowledgement

MRC

REFERENCES

1. Hurst GC, Henderson TA, Kreilick RW. *J. Am. Chem. Soc.* 1985; **107**: 7294.
2. Rist GH, Hyde JS. *J. Chem. Phys.* 1970; **52**: 4633.
3. Coremans JWA, Poluektov OG, Groenen EJJ, Canters GW, Nar H, Messerschmidt A. *J. Am. Chem. Soc.* 1994; **116**: 3097.
4. Coremans JWA, Poluektov OG, Groenen EJJ, Canters GW, Nar H, Messerschmidt A. *J. Am. Chem. Soc.* 1996; **118**: 12 141.
5. Yocum CF, Pecoraro VL. *Curr. Opin. Chem. Biol.* 1999; **3**: 182.
6. Horsburgh MJ, Wharton SJ, Karavolos M, Foster SJ. *Trends Microbiol.* 2002; **10**: 496.
7. Chang CH, Svedruzic D, Ozarowski A, Walker L, Yeagle G, Britt RD, Angerhofer A, Richards NGJ. *J. Biol. Chem.* 2004; **279**: 52 840.
8. Kalb (Gilboa) AJ, Habash J, Hunter NS, Price HJ, Raftery J, Helliwell JR. *Metal Ions in Biological Systems*, vol. 37. M. Dekker: New York, 2000; 279.
9. Reed GH, Poyner RR. *Metal ions in Biological Systems*, vol. 37. M. Dekker: New York, 2000; 183.
10. Malmström BG, Vänngård T, Larsson M. *Biochim. Biophys. Acta* 1958; **30**: 1.
11. Reed GH, Markham D. *Biological Magnetic Resonance*, vol. 6, Berliner LJ, Reuben J (eds). Plenum Press: New York, 1984; 73.
12. Deacon AT, Gleichmann T, Kalb (Gilboa) AJ, Price HJ, Raftery J, Brabbrook G, Yariv J, Helliwell JR. *J. Chem. Soc. Faraday Trans.* 1997; **93**: 4305.
13. Meirovitch E, Luz Z, Kalb AJ. *J. Am. Chem. Soc.* 1974; **96**: 7538.
14. Carmieli R, Manikandan P, Epel B, Kalb (Gilboa) AJ, Schnegg A, Savitsky A, Möbius K, Goldfarb D. *Biochemistry* 2003; **42**: 7863.
15. Carmieli R, Manikandan P, Kalb (Gilboa) AJ, Goldfarb D. *J. Am. Chem. Soc.* 2001; **123**: 8378.
16. Meirovitch E, Poupko R. *J. Phys. Chem.* 1978; **82**: 1920.
17. Kurreck H, Kirste B, Lubitz W. *Electron Nuclear Double Resonance Spectroscopy of Radicals in Solution*. VCH Publishers: Weinheim, 1988.
18. VardiR, BernardoM, ThomannH, StrohmaierKG, Vaughan DEW, Goldfarb D. *J. Magn. Reson.* 1997; **126**: 229.
19. Goldfarb D, Bernardo M, Strohmaier KG, Vaughan DEW, Thomann H, Poluektov OG, Schmidt J. *J. Am. Chem. Soc.* 1996; **118**: 4665.
20. Sturgeon BE, Ball JA, Randall DW, Britt RD. *J.Phys. Chem.* 1994; **98**: 12 871.
21. Grant CV, Ball JA, Hamstra BJ, Pecoraro VL, Britt RD. *J. Phys. Chem.* 1998; **102**: 8145.
22. Weil JA, Wertz JE, Bolton JR. *Electron Spin Resonance: Elementary Theory and Practical Applications*. John Wiley & Sons Inc., New York 1994; 304.
23. Manikandan P, Carmieli R, Shane T, Kalb (Gilboa) AJ, Goldfarb D. *J. Am. Chem. Soc.* 2000; **122**: 3488.
24. Habash J, Raftery J, Nuttall R, Price HJ, Wilkinson C, Kalb (Gilboa) AJ, Helliwell JR. *Acta Cryst.* 2000; **D56**: 541.
25. Arieli D, Prisner TF, Hertel M, Goldfarb D. *Phys. Chem. Chem. Phys.* 2004; **6**: 172.
26. Blok H, Disselhorst JAJM, van der Meer H, Orlinskii SB, Schmidt J. *J. Magn. Reson.* 2005; **173**: 49.